Chapter 4

Strain localization the brittle-viscous transition (Cap de Creus, NE Spain)

Fusseis, F., Handy, M.R.[1]

4.1 Abstract

Brittle and viscous deformation mechanisms interacted during the propagation of upper greenschist-facies mylonitic shear zones at the Cap de Creus, NE Spain. On a macroscale, decimeter long fracture-like discontinuities segment the metapsammitic and metapelitic host rocks in tip damage zones of mylonitic shear zones. On a microscale, these discontinuities were correlated to transgranular microfractures, which accommodate strain coevally with distributed dislocation creep in quartz and a deformation-induced reaction of biotite.

The relative contributions of the individual deformation mechanisms are strain-dependent. Initial straining is characterized by the formation of isolated extensional microfractures that interconnect to form transgranular microshears. Coeval distributed dislocation creep in quartz becomes more important during ongoing deformation, together with a reaction of biotite to

[1]This chapter is going to be submitted, in a slightly modified form, to *Journal of Structural Geology.*

form fine-grained aggregates of secondary biotite, muscovite, chlorite and ilmenite. After a critical shear strain of ∼1, these fine-grained neoblasts and dynamically recrystallized quartz together form a rheologically weak phase that accommodates all of the deformation. Transgranular microshears become inactive and their fault rock recrystallizes dynamically. We interpret this to represent a strain-dependent brittle-viscous transition.
It could furthermore be shown that the alinement and distribution of biotite in pre-existing cleavage domains deflects propagating microfractures. High contents of well-aligned biotite in contiguous cleavage domains at high angles to $\sigma 1$ promote propagation of right-lateral shear fractures within, or in orientations antithetically-rotated with respect to the shearing plane. We interpret these microscale effects to explain the macroscopically observed fracture tip geometries that were described by Fusseis et al. (2006).

4.2 Introduction

Heterogeneous deformation involves the formation of shear zones with subparallel walls in which deformation is localized (Ramsay, 1980). At the tips of shear zones, the progression of structures from the edges of the shear zone to its center provide a time sequence of development of structures within the shear zone (Mitra, 1984). Hence, terminations of such shear zones bear important information on deformation mechanisms involved in strain localization and the geometrical evolution of progressive deformation.

Terminations and nucleation of greenschist-facies shear zones were described by, e.g., Ramsay & Allison (1979), Simpson (1983), Segall & Pollard (1983), Segall & Simpson (1986), Tourigny & Tremblay (1997) and Mancktelow & Penacchioni (2005), mostly from granitic rocks. Most of these descriptions involve precursory brittle fracturing into shear zone propagation, where fracturing is ultimately triggered by stress rises that occur around the tips of shear zones (e.g. Schmid & Podladchikov, 2003, Mancktelow, 2006 for recent contributions). Fractures in the tip damage zones of mylonitic shear zones are supposed to enhance ductility and mylonitic deformation by increasing fluid fluxes and thereby promoting chemical softening and hydrolytic weakening (Segall & Simpson, 1986).

However, granitic rocks are mostly considered as mechanically isotropic on the meter- to decameter-scales. Descriptions of terminations of mylonitic

shear zones in layered, mechanically anisotropic rocks are rare. The effects of foliations or sedimentary layering on shear zone propagation have been investigated theoretically (e.g. Weijermars, 1992) and in analog and numerical experiments (e.g. Gottschalk 1990, Shea & Kronenberg, 1992, 1993, Kocher, 2005). Fusseis et al. (2006) described terminations of both, brittle and mylonitic shear zones from the Cap de Creus, NE Spain. They found that pre-existing foliations at high angles to the shearing planes are generally folded into what Elliott (1976) described as 'ductile beads', monoclinal folds that form ahead of the shear zone tip.

Fusseis et al. (2006) found that these monoclinal folds are mostly segmented by discrete discontinuities, which they interpreted as brittle fractures. Based on field observations, they suggested that progressive strain localization in these greenschist-facies shear zones was characterized by the coeval activity of brittle and viscous deformation mechanisms and that shear zone propagation at the Cap de Creus involves a strain-dependent brittle-viscous transition.

In this paper, we extend the outcrop-scale study of Fusseis et al. (2006) to the microscale. We demonstrate that the nucleation of mylonitic shear zones is closely related to the formation of brittle fractures on the grain- to the decimeter-scales and present microstructural evidence for their coeval activity with distributed dislocation creep at upper greenschist-facies conditions. We investigate the influence of an existing foliation on this processes and and conclude by presenting a microstructural model for the partitioning of strain among different deformation processes during strain localization and shear zone propagation.

4.3 Geological background

The pelitic and psammitic host rocks of the investigated shear zones experienced polyphase deformation during Variscan low-pressure/high-temperature metamorphism (Druguet, 2001, Carreras, 2001). At least two tectonometamorphic phases affected the rocks before (D1) and around (D2) peak metamorphic conditions. Sedimentary S0 was isoclinally folded during D1 to form S0/1. In the investigated area, a composite foliation S1/2 resulted from tight to isoclinal D2 folding of S0/1 and forms the dominant fabric element which is pre-existent to the formation of the D3 shear zones described below. The microscopic characteristics of S1/2 will be described in the next section. The pressure- and temperature-conditions in the investigated area have been estimated as up to 600°C/430MPa during D1 deformation, 670°C/470MPa (metamorphic peak) during D2 deformation and cooling from 560°C/240MPa to sub-greenschist facies conditions during D3 deformation (Druguet, 2001 and references therein).

Three different types of D3 shear zones can be distinguished in the investigated network. Each type is related to a specific deformation increment during the formation of the shear zone network and characterized by a unique appearance in the field.

1. *F-type shear zones* are centimeter-to meter-long fractures that formed during the initial increments of strain and played a key role in the propagation and widening of the mylonitic shear zones (red lines in Fig. 4.1). In the field, they appear as up to several meters long planar discontinuities that do not contain a macroscopically visible mylonite or fault rock (Fig. 3.4 in Fusseis et al., 2006).

2. Thin, decimeter- to several meters-long ultramylonitic *UM-type shear zones* are associated with the interconnection and widening of the shear zones (yellow lines in Fig. 4.1). In the field, these shear zones are usually characterized by their vein-like appearance. They contain a dark gray to black mylonite in which individual grains cannot be resolved using a hand lens. Often, these shear zones are not deflected by pre-existing fabrics.

3. *M-type shear zones* are the widest shear zones (meter-decameter scale) and accommodate the largest displacements (grey lines in Fig. 4.1).

In the field, they are characterized by a pronounced foliation S3 and stretching lineation L3. Individual grains can usually be resolved using a hand lens. They are the 'typical' Cap de Creus mylonites described in the literature (e.g. Carreras, 2001)

The D3 shear zones form the "Northern Shear Belt" that accommodated right-lateral transpression under retrograde, greenschist-facies conditions (Carreras, 2001 and references therein). To understand the evolution of these shear zones, this paper investigates strain localization in F-type shear zones and the strain-dependent transition to M-type shear zones. In the following Chapter 5, it is shown how UM-type shear zones form and the significance of the individual types of shear zones for the formation of shear zone networks is delineated.

4.4 The formation of isolated mylonitic (M-type) shear zones

Fusseis et al. (2006) observed that in ductile tip damage zones of mylonitic M-type shear zones deformation is partitioned into what they interpreted as discrete brittle fractures (F-type shear zones) and distributed shearing between these fractures (Fig. 4.2). They interpret the progression of structures from the edges of the tip damage zone to the shear zone center as a time sequence of the development of structures and interpret strain localization to be initiated by fracturing and segmentation of S1/2 ('1' and '2' in Fig. 4.2). Closer to the shear zone center, brittle segmentation coincides with the deflection of S1/2 in a ductile bead (Elliott, 1976, '3' in Fig. 4.2). Increasing deflection of S1/2 and pronounced thinning of individual sedimentary layers mark the establishment of a mylonitic M-type shear zone that accommodates all of the imposed displacement ('4' in Fig. 4.2). Fusseis et al. (2006) interpreted this progression of structures as a strain-dependent brittle-viscous transition. In the following we will describe the microstructural evolution of this transition as deduced from metapsammitic, metapelitic and Qtz-vein samples that were collected in tip and lateral damage zones of the shear zones (Fig. 4.2).

Mineral names used in the text are abbreviated as follows: quartz - Qtz, biotite - Bt, muscovite - Ms, chlorite - Chl, plagioclase - Plag, feldspar - Fsp, ilmenite - Ilm, sillimanite - Sil, tourmaline - Tur. Supplementary

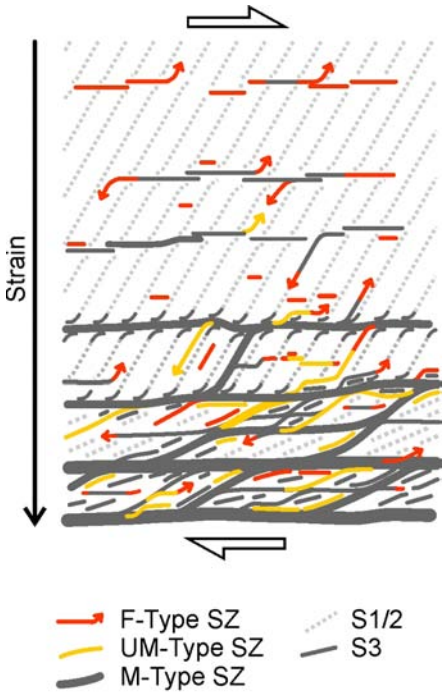

Figure 4.1: Schematic model of shear zone networking after Fusseis et al. (2006). Three types of shear zones are distinguished according to dominant deformation mechanism and their relative role in shear zone networking: F-type shear zones (red) deform by fracturing and are involved in initial strain localization as well as in growth of UM-type and M-type shear zones. UM-type shear zones (yellow) deform predominantly by grain size-sensitive creep and contribute to shear zone interconnection and widening of M-type shear zones. M-type shear zones (grey) form the widest shear zones and deform predominantly by dislocation creep.

numbering of these abbreviations refers to the generations of these minerals (eg. Qtz1 - quartz, first generation). For sample descriptions see App. 9.3, for sample locations see Fig. 4.2 and App. 9.3. Microstructures were studied in standard thin sections (25μm thick) using a polarisation microscope (Leica DMLP). Scanning electron microscopy was done using a JEOL JSM6300 device.

4.4.1 Fabrics in unsheared rocks

In thin section, S1/2 in metapsammites is characterized by alternating microlithons and cleavage domains (Passchier & Trouw, 2005). Microlithons

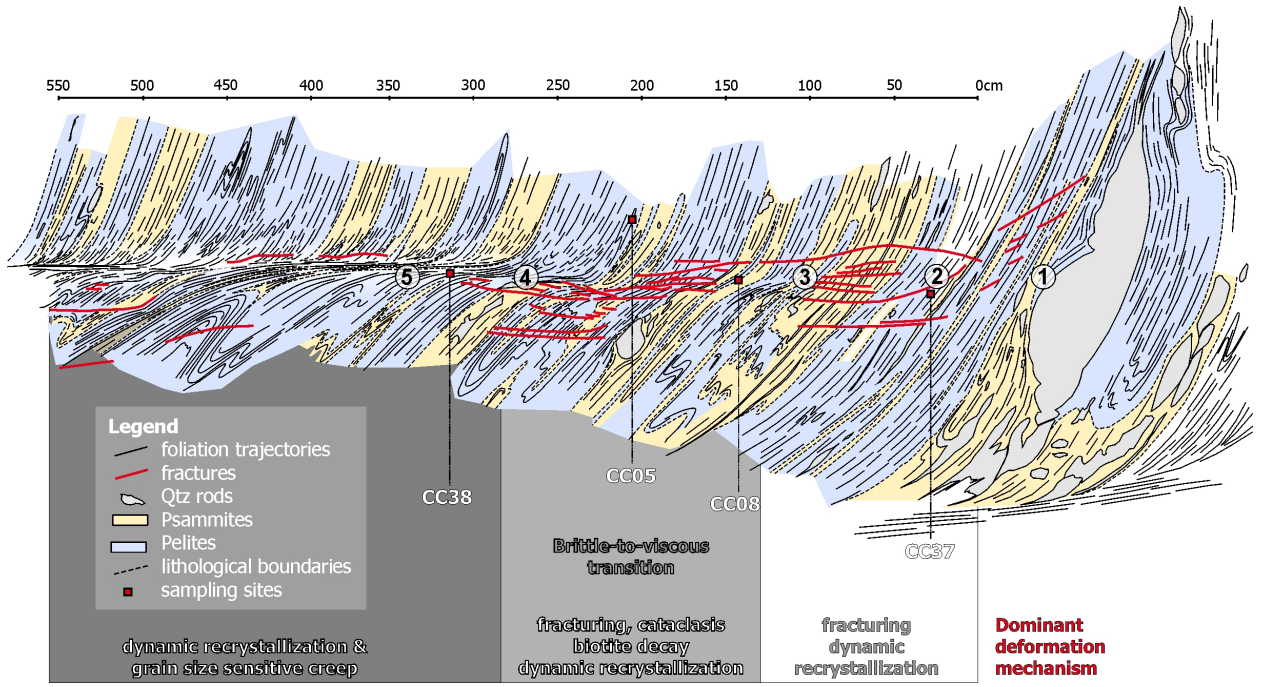

Figure 4.2: Termination of a mylonitic M-type shear zone in the Cala Prona. See text for explanation. Note sampling sites of samples CC05, CC08, CC37 and CC38. The sketch map is approximately parallel to the stretching lineation and perpendicular to the mylonitic foliation in the shear zone. View towards ENE. UTM 31T 521767 east, 4687430 north.

are defined by Qtz1 and Plag1, cleavage domains are dominated by aligned Bt1, minor Ms1 and secondary Chl (Fig. 4.3). These cleavage domains may form a pronounced disjunctive foliation (Fig. 4.3) or are transitional, with increasing mica-content, to a continuous foliation in metapelites. In metapelites, S2 is defined almost solely by Bt1 aligned parallel to the axial planes of relict millimeter to centimeter-scale isoclinal F2 folds. The main constituent minerals in both, metapelites and metapsammites, are Qtz and Bt, Plag and Ms (App. 9.3). Qtz1 in sample CC05 shows minor undulatory extinction and few subgrains (Fig. 4.3). Bt1 shows reaction rims where Bt2 and Ilm form (Fig. 4.3). Ms1 mostly occurs as millimeter-sized clasts that overgrew S1/2 in arbitrary orientations. Plag (An 20 to 35%) does not form interconnected layers and therefore is inferred not to have affected the bulk rheology. The deformation state of sample shown in Fig. 4.3 corresponds roughly to what has been described as the 'least-deformed' state that can be found at the northern part of the Cap de Creus (Garcia-Celma, 1983).

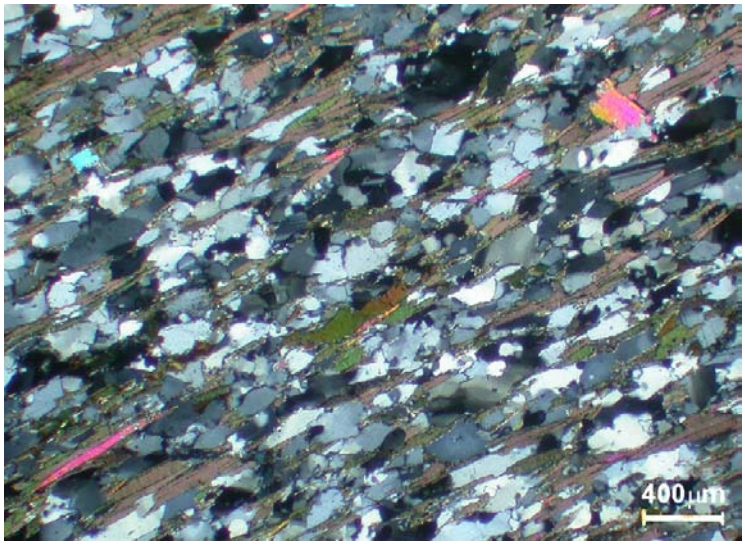

Figure 4.3: Sample CC05, collected at the lateral margin of the damage zone of the shear zone in Fig. 4.2. The sample shows a minor mylonitic overprint. Note aligned Bt1 in cleavage domains forming a disjunctive foliation S1/2. Bt shows reaction rims. Qtz exhibits minor undulatory extinction and dynamic recrystallization. Ms overgrows S1/2 (bright orange interference colours, in upper right corner).

4.4.2 Distributed deformation

Within the tip damage zones of the investigated shear zones the significance of distributed deformation increases from the margin of the damage zone towards the shear zone center. It is accommodated by the main constituent minerals Qtz1 and Bt1 and, to a lesser degree by Plag1 and Ms1.

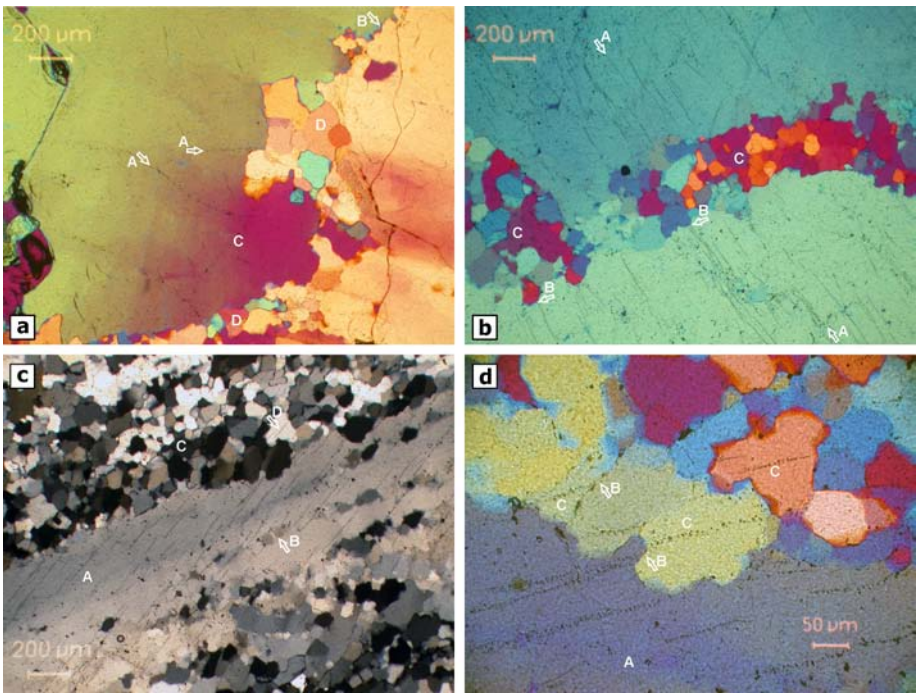

Figure 4.4: FIPs, dynamic recrystallization and healed microshears (1/2). Samples CC11a (a, b) and CC11c (c, d) (a) Qtz1 grain boundary. Note FIPs ('A'), bulges ('B'), sweeping undulatory extinction ('C') and dynamically recrystallized grains ('D'). (b) FIPs in Qtz1 grains ('A'). FIPs terminate at the boundaries with dynamically recrystallized grains ('B'). (c) Qtz1 ribbon grain ('A') transected by numerous FIPs ('B'). Most Qtz1 is dynamically recrystallized by grain boundary bulging and subgrain rotation ('C'). Short segments of FIPs are preserved in some of the dynamically recrystallized grains ('D'). (d) Detail from (e). The Qtz1 ribbon grain is transected by FIPs ('A'), which are displaced across the grain boundaries towards the dynamically recrystallized grains ('B'). Short segments of FIPs are preserved in some of the dynamically recrystallized grains ('C'). Crossed polarizers, a, b, d with gypsum plate inserted. XZ-sections. See Appendix 1 for sample location.

The progressive deformation of Qtz1 commences in samples from the outermost parts of damage zones by the formation of sweeping undulatory extinction and deformation bands (Fig. 4.4). Individual Qtz grains that are

suitably oriented for dislocation glide form ribbons (Figs. 4.4c and 4.6a). Increasingly strained Qtz1 recrystallizes by grain boundary bulging and forms mantles of Qtz2 (Figs. 4.4a and b). Even higher strains give rise to subgrain rotation recrystallization ('A' in Fig. 4.5a). The grain size of the dynamically recrystallized grains is in the range of 60-90 μm.

Bt1 in damage zones deforms by basal glide, pressure solution and minor kinking, all of which are typical deformation mechanisms for biotite at greenschist-facies conditions (Fig. 4.6a, e.g. Kerrich et al., 1980, 1981, Shea & Kronenberg, 1992, Shea et al., 1993). At all of these microstructural sites and along its grain boundaries, Bt1 has fine-grained (20-50 μm) mantles consisting of Bt2, Ms2, Ilm, and Chl (Figs. 4.6b and c). These have been described by Kerrich et al. (1980, 1981) as reaction fabrics; the reaction was interpreted as deformation-catalyzed. The proportion of reaction products increases towards the center of the shear zone. In sample CC08 (Figs. 4.6b and c) the recrystallized grains form an interlocked and undeformed groundmass with grain sizes $< 100\mu$m. With increasing shear strain (i.e. closer to the shear zone center) reaction products in the matrix become aligned parallel to S3 (Figs. 4.13).

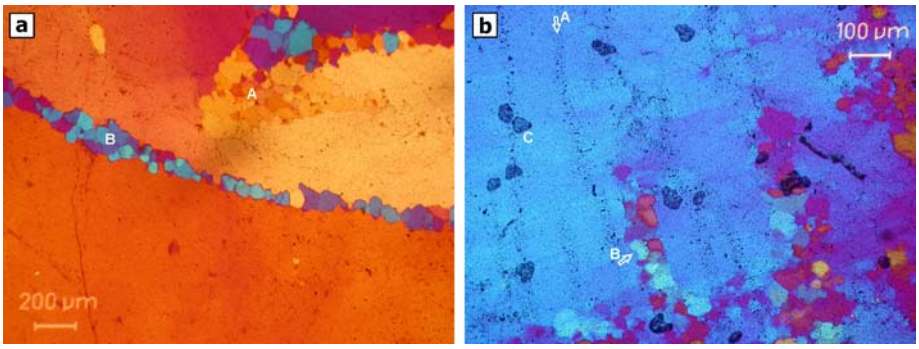

Figure 4.5: FIPs, dynamic recrystallization and healed microshears (2/2). Sample CC11b (a) Qtz1 grain dynamically recrystallizing by subgrain rotation ('A'). Array of recrystallized grains within the host grain shows a systematic difference in crystallographic orientation ('B'). (b) Subparallel FIP ('A') and array of dynamically recrystallized grains ('B'). 'C' are air bubbles resulting from sample preparation. Crossed polarizers, both with gypsum plate inserted. XZ-sections. See Appendix 1 for sample location.

Porphyroclastic Ms1 is often boudinaged by transgranular microshears (see below, Figs. 4.7a, b and 4.13b). Ms1 clasts whose basal planes are oriented at high angles to S1/2 develop kink folds parallel to S1/2 with Bt,

Chl and Plag growing in the axial planes (red arrows in Fig. 4.7c and 'D' in 4.7c). This kinking may indicate D3 shortening perpendicular to S1/2.

Plagioclase clasts are polysynthetically twinned and often fractured. Twin lamellae are occasionally bent. Near shear fractures, Plag generally underwent retrograde reaction to white mica, betraying the former presence of fluid ('B' in Fig. 4.8b).

4.4.3 Intragranular scale strain localization

Microfractures and their healed remnants, fluid inclusion planes (FIPs, Anders & Wiltschko, 1994, Lespin-ase, 1999, Boullier, 1999), are common features in samples from the most external parts of ductile damage zones and preferentially crosscut Qtz1 and Plag1 porphyroclasts ('A' in Figs. 4.4a-d and 4.5b and Fig. 4.8a and c). Most of them are orientated at high angles to S1/2 and terminate at aggregates of dynamically recrystallized grains (Figs. 4.4c). FIPs are most frequently found in larger (i.e. $>500\ \mu$m) grains and can occasionally be traced across grain boundaries. The least-deformed quartz samples contain several crosscutting generations of intragranular FIPs.

No FIPs were found in dynamically recrystallized quartz (Qtz2) grains, except in the immediate neighborhood of ribbon grains (Fig. 4.4c and d). FIPs can occasionally be traced from ribbon grains into neighboring Qtz2, where they form short segments and are often slightly displaced or tilted across the grain boundaries towards the ribbon grains (Fig. 4.4c and d). No FIPs are preserved further than about two grain diameters away from the ribbon grains.

Microfractures and FIPs are typically related to arrays, or 'strings' of dynamically recrystallized grains or subgrains in otherwise less deformed parental Qtz1 grains (Figs. 4.5a&b, and Figs. 4.8a, b and 4.9b). Grains forming these arrays usually have markedly different crystallographic orientations than their parental grains and are isolated from subgrains in the host grains ('B' in Fig. 4.5a, arrow 'B' in Fig. 4.8a). FIPs were found ahead of the tips of such arrays (Fig. 4.5b).

Evidence that microfracturing preceded the formation of dynamically recrystallized grains forming the arrays comes from sample CC14. There, several microfractures were found crosscutting a Qtz1 microlithon (arrows 'A', 'B' and 'C' in Fig. 4.8a). Subgrains formed in the plane of the microfractures and in arrays parallel to them ('B' and 'C' in Fig. 4.8a). Along

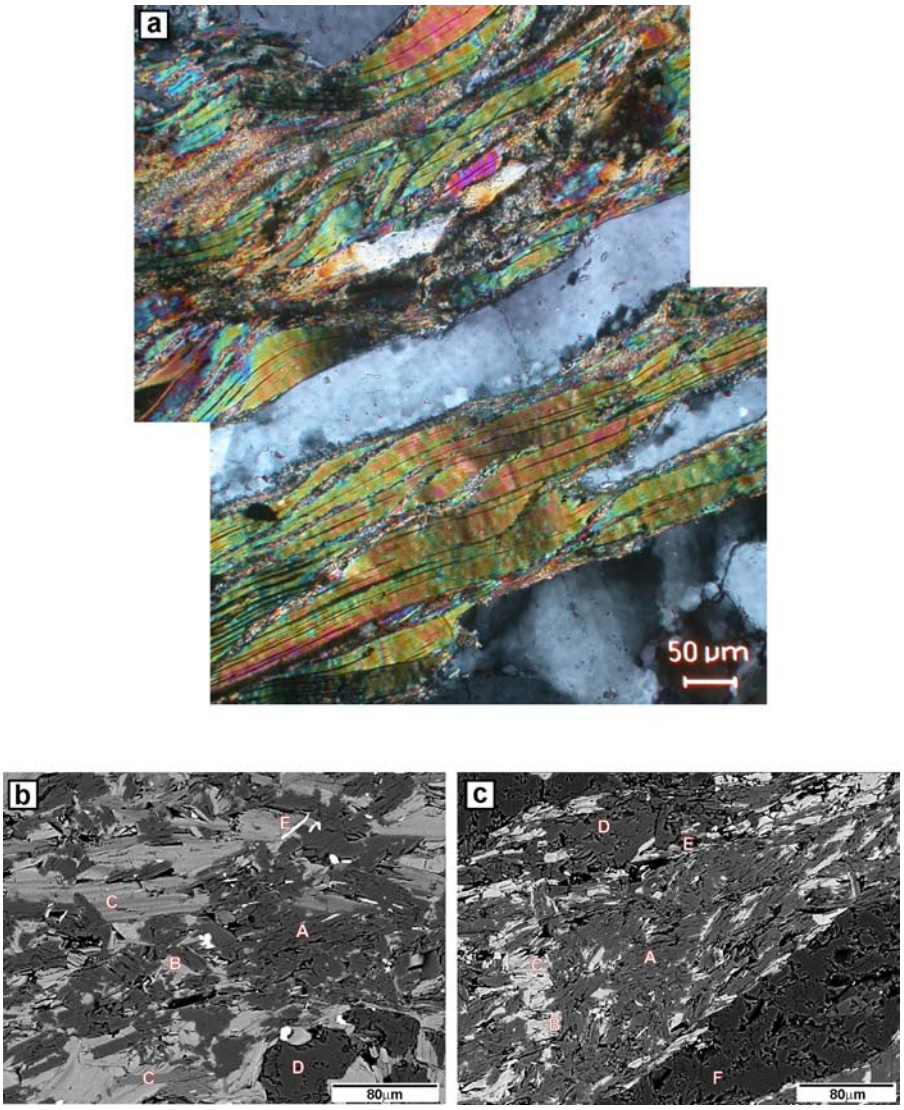

Figure 4.6: (a) Bt deformation in sample CC17a collected from an ultramylonitic shear zone in Cala Serena. Bt deformed predominantly by basal glide, bending and pressure solution. Neocrystallized mantles consist of Bt2, Ms2, Ilm and Chl. Note Qtz ribbon between the two Bt aggregates. Qtz deforms by dislocation glide, grain boundary bulging and subgrain rotation recrystallization. See text for explanation. (b&c) Fine grained, undeformed aggregates of neocrystallized minerals in sample CC08 consisting of Bt2, Ms2, Ilm, Chl and minor Plag. Recrystallized phases (except Plag) result from deformation-induced decay of Bt1. 'A' - Ms, 'B' - Bt, 'C' - Chl, 'D' - Plag, 'E' - Ilm, 'F' - Qtz. See text for explanation.

the central microfracture, the subgrains only decorate a short segment of the microfracture ('B' in Fig. 4.8a). Sweeping undulatory extinction in the segmented host grain terminates against the microfractures (Fig. 4.8a), evidencing that the microfracture hindered dislocation movements (see discussion).

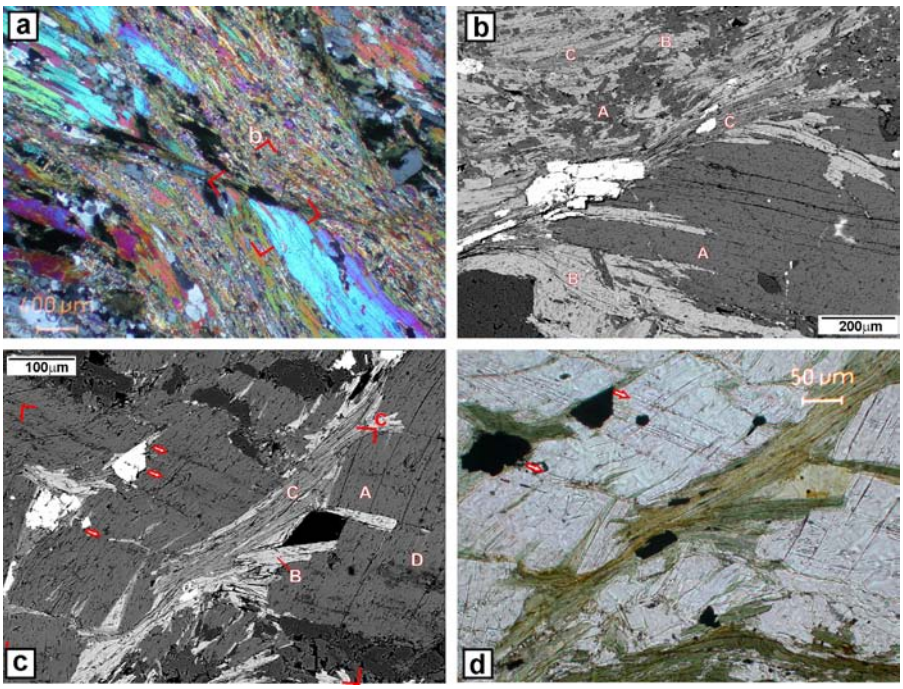

Figure 4.7: Shear bands from sample CC08. (a) Micrograph showing Ms porphyroclast, transected by a sinistral shear band. Note fine-grained newly grown aggregates above and below the shear band. S1/2 oriented NW/SE in the thin section. (b) Detail from (a). 'A' - Ms, 'B' - Bt, 'C' - Chl. BSE image. (c) BSE image of boudinaged Ms porphyroclast, basal planes Ms are oriented almost 90° to S1/2 (oriented E/W). Note kink bands in the Ms (red arrows). (d) Micrograph, detail from (c). Mineral phases labeled as in (b). See text for explanation and Fig. 4.2 for location.

4.4.4 Strain localization on the transgranular scale

D2 fabrics in the damage zones of metapsammitic, mylonitic shear zones are usually segmented by planar discontinuities some 2 - 3 cm long. These discontinuities are generally parallel to decimeter-long shear fractures in the outcrop (Fig. 4.2). In thin sections, they were found to displace grain boundaries and are therefore identified as shear fractures ('microshears',

displaced Plag 'B' in Fig. 4.8b, Ilm displaced by microshear 4-4' in Fig. 4.8c).

Transgranular microshears more than 1mm long and up to $\sim 200\mu m$ wide often occur in longitudinal arrays. In mica-rich samples, transgranular microshears form shear bands displacing S1/2 (Figs. 4.7 and 4.11). The amount of shear bands increases towards the mylonitic shear zone center. Transgranular microshears tend to crosscut S1/2 at angles between 30° and 80° (Figs. 4.8 and 4.9). Close to their termination they appear in a step-like geometry, deflected in cleavage domains but crosscutting Qtz/Fsp microlithons at about 30° with respect to S1/2 (Fig. 4.10).

FIPs were found parallel to terminations of transgranular microshears, which indicates that the formation of transgranular microshears was preceded by smaller-scale microfractures. Fig. 4.8c shows FIPs ('C' in Fig. 4.8c) in a Plag parallel to a transgranular microshear (4-4' in Fig. 4.8c) displacing a string of Ilm that formed along the margins of a Bt grain ('A' in Fig. 4.8c). Intragranular fractures ('A', 'B' and 'C') linking two transgranular microshears in Fig. 4.8a (1-1' and 2-2', both longer than the shown cutout) may represent precursory stages of microshear formation and would then support this interpretation.

Transgranular microshears are often decorated by newly grown mica and other, unidentified minerals (Figs. 4.8c ('B') and 4.9a). Where crosscutting Qtz1, transgranular microshears can be traced by arrays of dynamically recrystallized Qtz2 as described above (arrow 'A' in Fig. 4.8b, arrow 'A' in Fig. 4.9b). Where they become several millimeters to centimeters long, transgranular microshears contain a polymineralic fault rock with Bt2, Ms2, Ilm, minor secondary Chl and Qtz2 and Plag2 in varied amounts (Figs. 4.11, 4.12).

Grains size decreases abruptly from the host minerals to the fault rock in microshears and the distribution of minerals in the fault rock is heterogeneous (Figs. 4.11, 4.12). The boundaries between fault rock and host rock are uneven and interpenetrating (Fig. 4.12c). Grains in microshears are between 30-150 μm in size and thus generally smaller than subgrains in dynamically recrystallized host grains and about two orders of magnitude smaller than the host grains themselves (Figs. 4.11, 4.12b-d). All tabular or columnar minerals are aligned parallel to the boundaries of the microshears (Figs. 4.12b and d). The formation of the polymineralic fault rock is am-

biguous. Yet, all of the minerals described along the transgranular fractures and microshears are clearly second-generation, which indicates syntectonic nucleation and growth in the microshears.

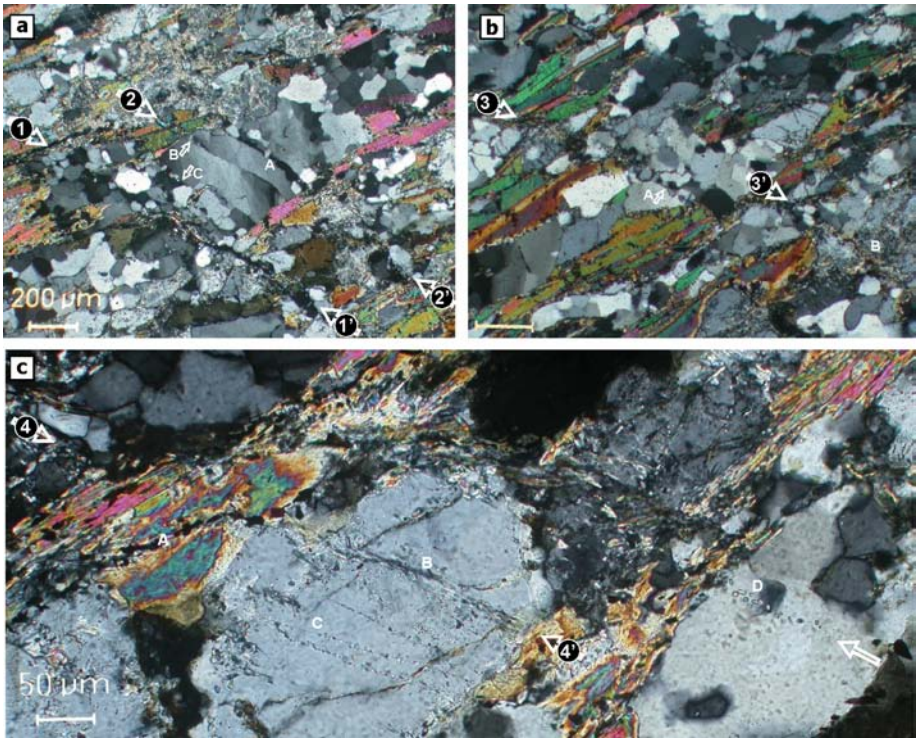

Figure 4.8: Microshears, FIPs and planar arrays of recrystallized grains from ductile tip damage zone in Cala Serena (1/2). Sample CC14. (a) Contractional stepover between two microshears (1-1' and 2-2'). Note intragranular microfractures and recrystallized grains in central Qtz-microlithon ('A', 'B' and 'C'). (b) Transgranular microshear (3-3') crosscutting and offsetting a microlithon ('A') and Plag ('B'). (c) Microshear (4-4') crosscutting Bt, Plag and Qtz grains. Note displaced Ilm-trail ('A'), small mica in microshear plane ('B'), FIPs ('C') and crystallized inclusions ('D'). Crossed polarizers.

4.5 Discussion

4.5.1 Combined fracturing and mylonitic shearing

The basic scope of this paper was to investigate the proposed coeval activity of brittle fracturing and mylonitic shearing that is interpreted to characterize strain localization in tip damage zones of mylonitic M-type shear zones (Fusseis et al., 2006). However, Fusseis et al. (2006) based their models on

field observations and inferred that the planar discontinuities they mapped in these damage zones formed as brittle fractures. Yet, the following questions arise: (1) Are the crack-like discontinuities (F-type shear zones) observed in outcrop (F-type shear zones) and interpreted as critical for strain localization in mylonitic (M-type) shear zones really fractures that resulted from brittle failure? (2) If the F-type shear zones formed by fracturing, what microstructural evidence indicates the relative timing of crack formation with respect to the mylonitic overprint of the rock?

Evidence from fluid inclusion planes and intragranular microfractures

The smallest microstructures indicative of brittle failure associated with strain localization in M-type shear zones are intragranular mode I microfractures and their healed remnants, fluid inclusion planes (FIPs, Figs. 4.4, 4.5, 4.8 and 4.9, Anders & Wiltschko, 1994, Lespinase, 1999, Boullier, 1999). Fluid inclusions evidence the presence of fluids in the rock (Roedder, 1984). The nature and origin of the fluids are not clear. However, the existence of cross-cutting FIPs suggests that brittle failure was accompanied by, perhaps even induced by, local fluctuations in fluid pressure and/or differential stress (Lespinase, 1999).

Indication that FIPs and thereby microfractures formed prior to or coeval with mylonitization comes from the observation that both are restricted to Qtz1 and do generally not occur in dynamically recrystallized Qtz2 grains. Lobate grain boundaries typical for Qtz2 grains indicate grain boundary bulging (Fig. 4.4d, e.g. Stipp et al., 2002), which is an effective mechanism to drain FIPs and transform microcracks into grain boundaries and leave behind inclusion- and fracture-free grains (Kerrich, 1976, Wilkins & Barkas, 1978, Urai, 1983, Urai et al., 1986, Bakker & Jansen, 1990, 1994). This fits our observations from dynamically recrystallized grains neighboring Qtz1 ribbon grains (Fig. 4.4c and d).

Evidence for microfracturing preceding mylonitization comes from small-scale microfractures linking two, millimeter-long transgranular microshears in sample CC14 (Fig. 4.8a). The undulatory extinction patterns cannot be correlated across the central fracture (arrow 'B'), which indicates that dislocation movements in both fragments occurred independently. The crack itself, which is decorated with unidentified tabular minerals, obviously hin-

ders dislocation movement and can therefore be interpreted as existent before dislocation movement ceased.

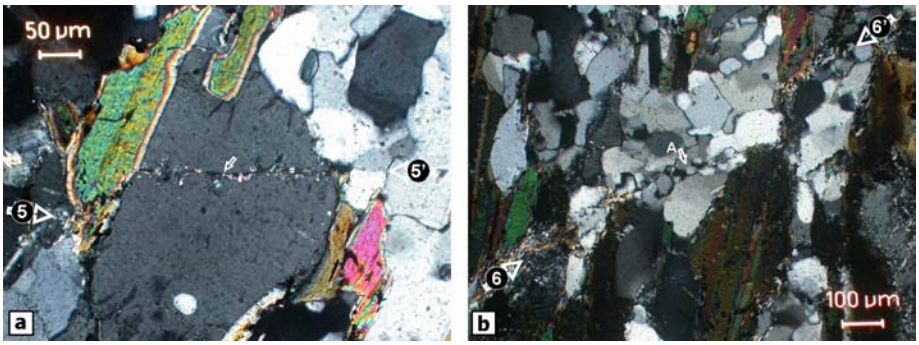

Figure 4.9: Microshears, FIPs and planar arrays of recrystallized grains from ductile tip damage zone in Cala Serena (2/2). Sample CC14. (a) Transgranular microfracture (5-5'), crossing a Qtz grain. Note newly crystallized phases decorating the microfracture (arrow). (b) Transgranular microshear (6-6') crossing a Qtz microlithon. Shearing plane is traced by small recrystallized grains (arrow). Crossed polarizers.

The formation of fault rock in microshears

Fluid inclusion planes in the direct prolongation of, or parallel to planar arrays of subgrains in Qtz1 (Fig. 4.5b) indicate a linked evolution of microfractures and subgrains. We argue that the arrays of dynamically recrystallized subgrains, which decorate intra- and transgranular microfractures in Qtz1, could be best explained by a combination of microcataclasis and subsequent dynamic recrystallization of the crystal fragments (Simpson, 1986, Lloyd & Knipe, 1992, den Brok et al., 1998, van Daalen et al., 1999, Trepmann & Stöckhert, 2003, Vernooij et al., 2006). The arrays were found relatively isolated within less-deformed host grains (Figs. 4.5a, 4.8b and 4.9b) and the size of the grains forming the array is usually smaller than those of distributes subgrains in the host grains (Figs. 4.8b and 4.9b), which suggests an evolution independent from distributed mylonitic microstructures in the host grains.

Simpson (1986) proposed a model for microcataclasis involving the interaction and interconnection of propagating microfractures which could explain the isolated position of the arrays as well as the small subgrain sizes. The often common misorientation of dynamically recrystallized grains in the arrays (Fig. 4.5a) may result from rigid body rotation of crystal fragments

(van Daalen et al., 1999). Dynamic recrystallization subsequent to cataclasis and slip might have modified cataclastic grain size distributions (Figs. 4.5 and 4.12).

Lack of a continuous evolution from deformation bands, via subgrains to the dynamically recrystallized grains forming the actual arrays indicates that they did not form by progressive subgrain rotation recrystallization (arrow 'B' in Fig. 4.8a, White, 1976, 1977, Urai et al., 1986, Drury & Urai, 1990). Bulging of intragranular microfracture planes (Urai 1983) or pinning of migrating dislocations by fluid inclusions could have caused the formation of these arrays at sites of earlier microfracturing, but cannot explain their often significant misorientation with respect to both adjacent crystal fragments (Fig. 4.5a) since grains resulting from bulging recrystallization generally inherit the crystallographic orientation of their parental grain (e.g. Stipp et al., 2002).

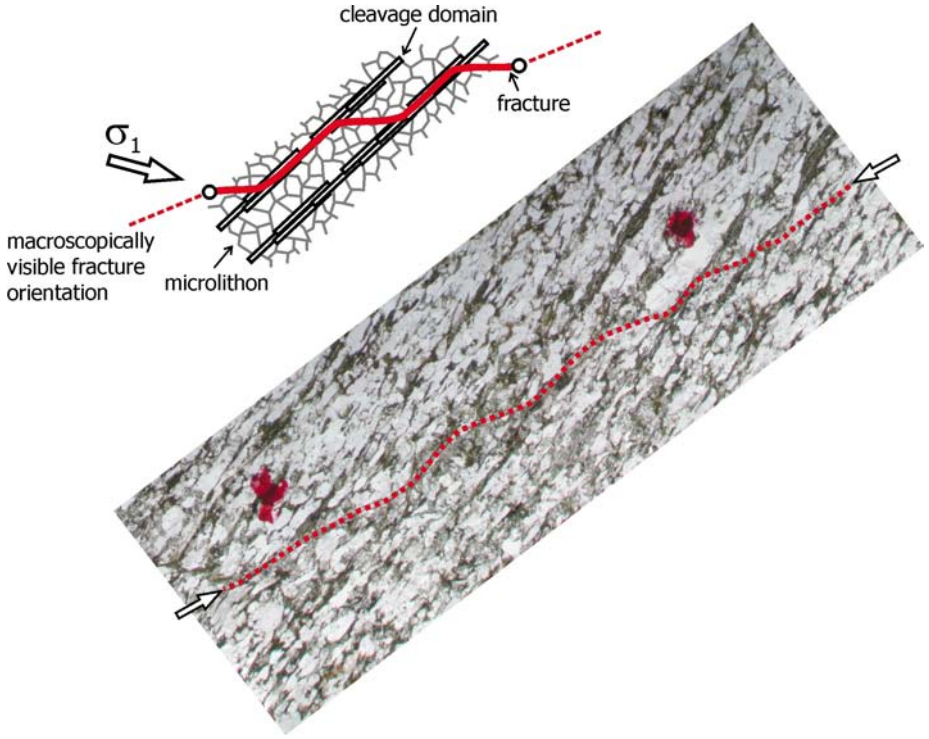

Figure 4.10: Termination of a transgranular microshear from sample CC037/1. Red stippled line traces microshear. See text for explanations.

In our interpretation, the formation of *polyphase* fault rock is also re-

lated to a combination of fragmentation of host grains by interacting and interconnecting microfractures as well as a preferred neoblastesis of products that result from the decay of Bt1. Bt2, Ms2, Ilm and Chl form fine-grained mantles around Bt1 but also the most common components in polyphase fault rock (Figs. 4.4, 4.5 and 4.12). Fluids that accomplish the necessary mass transport during the reaction and circulate in the rock should be attracted by nearby fractures, which represent sites of low effective pressure. Low effective pressures decreases the solubility of chemical phases in the fluid, promoting an enhanced precipitation (e.g. Durney & Ramsay, 1973, Ramsay, 1980). Neoblastesis of minerals along microfractures is often observed in the investigated samples ('B' and 'D' in Fig. 4.8c and arrow in Fig 4.9a). Isometric Qtz2 and Plag2, which also form considerable portions of the polyphase fault rock (Fig. 4.11), may result from fragmentation of Qtz1 and Plag1 by interacting microfractures as described above.

The distribution and alignment of minerals in the investigated microshears can be best explained by granular flow and diffusion-assisted healing (Figs. 4.11 and 4.12). The latter, occurring subsequent to slip might explain the jagged boundaries between the microshears and the host grains and should have obscured all traces of abrasive wear during slip (Figs. 4.11 and 4.12). The alignment of the Bt2, Ms2, Chl and Ilm indicates dynamic recrystallization of the fault rock within a uniform stress field.

Based on these observations we conclude that transgranular microshears are the thin section-scale equivalents of the decimeter-long discontinuities observed in the outcrop (Fig. 2, Figs. 3 and 4 in Fusseis et al., 2006). These discontinuities did form by brittle failure and are therefore correctly termed fractures (Fusseis et al., 2006).

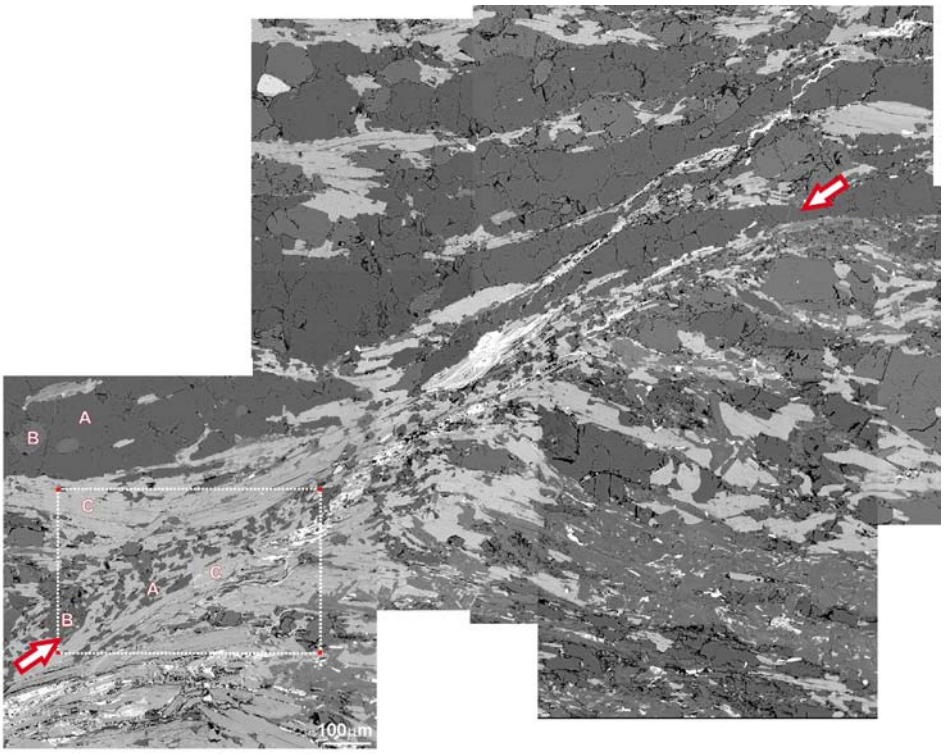

Figure 4.11: Shear band from metapelitic part of sample CC37/2. Note dynamically recrystallized grains of Qtz2, Plag2 and Bt2 in center of the shear band and minor deflection of Bt1. Dotted rectangle marks position of the element distribution maps in App. 9.3. 'A' - Qtz, 'B' - Plag, 'C' - Bt. See text for explanation.

4.5.2 Fracture propagation and the role S1/2

Several studies have shown that mylonitic shear zones can evolve from brittle fractures (e.g. Segall & Simpson, 1986, Simpson et al., 1982, Tourigny & Tremblay, 1997, Guermani & Pennacchioni, 1998, Penacchioni, 2005, Mancktelow & Pennacchioni, 2005). In most cases such shear zones have inherited the orientation of the initial fractures. Fusseis et al. (2006) note that the precursory fractures in tip damage zones of mylonitic shear zones are either parallel to the mylonitic shear zone center (see stereoplot in Fig. 5 in Fusseis et al. 2006) or formed up to 90° anticlockwise rotated with respect to the D3 dextral shear zones (see Fig. 2 in Fusseis et al., 2006). However, fractures in both orientations are difficult to explain as having evolved in a common stress field with the mylonitic shear zones. Tip damage zones of natural shear fractures are usually characterized by tensional fractures parallel to

the $\sigma 1$ direction, such that the resulting fractures form rotated synthetically (clockwise) with respect to the right-lateral shearing plane (Scholz et al., 1993, McGrath & Davison, 1995, Vermilye & Scholz, 1998) .

A solution to this problem may be found by considering the effect of the existing foliation S1/2, which represents a major mechanical anisotropy. The compressive strength of mechanically anisotropic metasedimentary layers depends on the angle β between $\sigma 1$ and S1/2. Strength anisotropy due to existing foliations has been extensively investigated in deformation experiments (e.g. Gottschalk et al., 1990, Shea & Kronenberg, 1992, 1993 and references cited therein) and is generally quantified with an anisotropy coefficient defined as the ratio of compressive strengths normal and at 45° to S [$\sigma d(90°)/\sigma d(45°)$]. Anisotropy coefficients for micashists range between 1 and 4, depending on mica content and distribution.

In the investigated metapelites and metapsammites S1/2 is defined by varying proportions of cleavage domains and microlithons characterized by the predominance of Bt1/Ms1 and Qtz1/Plag1 respectively. The amount and distribution of these minerals, especially Bt and Qtz, control the strength anisotropy and therefore the rheological behaviour of the metasediments, but also influence fracture propagation (e.g. Shea & Kronenberg, 1993). In the investigated samples, S1/2 clearly influences the orientation of transgranular microshears near their terminations: Tip segments of microshears are deflected by foliation-parallel Bt in cleavage domains, whereas they cut through microlithons at angles of ∼40° to S1/2 (Fig. 4.10). The deflection of propagating fractures in cleavage domains results in stepped geometries of fracture tips. The length of microlithon- and cleavage domain segments is related to the anisotropy of the microfabrics: the thicker the mica layers, the better the alignment of the micas and the greater their contiguity, the longer the cleavage domain segments. Central fracture segments are flat, suggesting that abrasive wear has smoothed the fracture plane.

Stepped fracture surfaces have been reported from experimentally deformed mica-rich samples by Gottschalk et al. (1990) as well as Shea & Kronenberg, (1993). These stepped fractures form largely independent of the shortening direction if $\beta \geq 45°$. According to Shea & Kronenberg, (1993), fracture segments transecting microlithons in all their investigated samples tend to form as tensional fractures at angles to $\sigma 1$ ranging from 0-20° and are connected by fracture segments that are parallel to mica aligned in cleav-

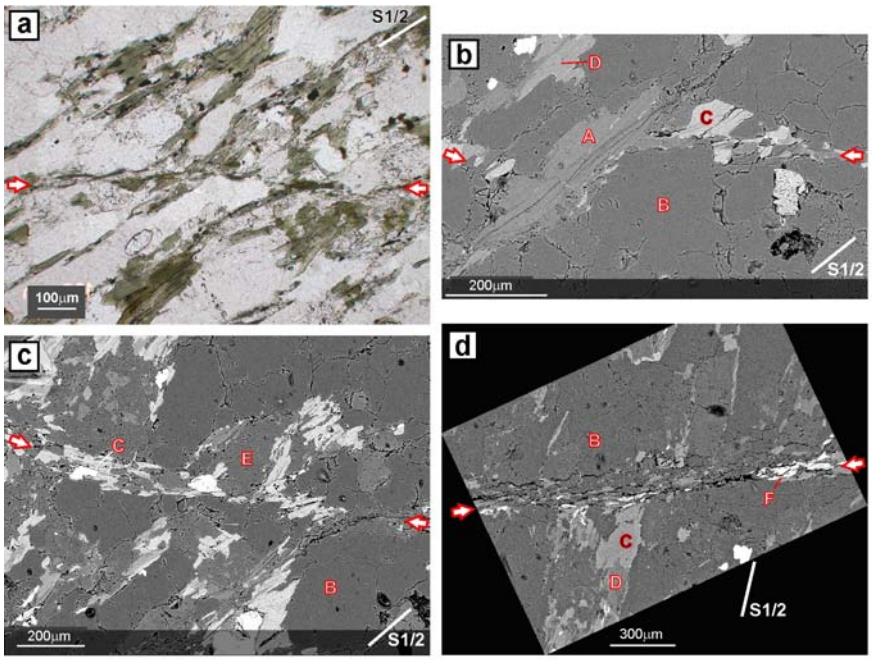

Figure 4.12: Transgranular microshears (indicated by white arrows). Metapsammitic part of sample CC37/1. (a) Microshear transecting S1/2. Note alignment of dynamically recrystallized minerals in the microshear. (b) Microshear offsetting the left margin of Ms porphyroclast which is aligned parallel to S1/2 ('A'). Note the small dynamically recrystallized minerals defining the microshear. 'B' - Qtz, 'C' - Bt, 'D' - Chl. BSE image. (c) Transgranular microshear defined by aligned Bt and equigranular Qtz. Labeling as in (c), 'E' - Plag. BSE image. (d) Transgranular microshear crosscutting S1/2. Note difference in grain size between host rock and the microshear. Labeling as in (c), 'F' - Ilm. BSE Image. See Fig. 4.2 for location.

age domains. The authors report fracture segments that follow S in cleavage domains from experiments that were shortened at angles β as high as 70-90°! Furthermore, they observed that stepped fractures form by the propagation and coalescence of microcracks that nucleated in quartz and feldspar.

These results of Gottschalk et al. (1990) and Shea & Kronenberg, (1993) explain why fractures in tip damage zones of mylonitic (type 3) shear zones propagate parallel to or even anticlockwise-rotated with respect to the shear zone center (Fig. 4.2) : The orientation of the propagating fracture is a function of the relative lengths of its cleavage-domain and microlithons segments (sketch in Fig. 4.10). High mica-content and contiguity in metapelites result in longer cleavage domain segments and therefore promote anticlock-

wise propagation of fractures in ductile beads (Fig. 4.2 and 4.10) where S1/2 rotates synthetically from its undeflected orientation (about 90° to the shearing plane) to parallelism with the shearing plane (Fig. 2, Figs. 3 and 4 in Fusseis et al., 2006). This explains our field observations that fractures in metapelites, which are characterized by extremely well defined cleavage domains, propagate in orientations up to 90° anticlockwise with respect to the D3 shearing plane (Fig. 3 in Fusseis et al., 2006). Furthermore it explains why the antithetic deflection of the propagating fracture is most pronounced at the external parts of ductile tip damage zones, where S1/2 is oriented at higher angles to the shearing plane (Fig. 4.2). Wider microlithons in deflected metapsammites (which result in longer microlithons segments of propagating fractures, Fig. 4.10) and/or a more acute angle between S1/2 and the shearing plane within ductile beads closer to the shear zone center advance fracture propagation parallel to the shearing plane (Fig. 4.2).

4.5.3 A model for the strength evolution of a mylonitic shear zone at the BVT

The following model is presented for the strength evolution of a mylonitic M-type shear zone propagating in a foliated rock whose rheology is governed by Qtz and aligned Bt. The strength of the rock changes with the evolution of microstructures during progressive strain localization, from undeformed host rock ahead of the shear zone, through the tip damage zone, to the mylonite in the center of the shear zone (Fig. 4.13).

The host rock outside of the damage zone is stressed to a background level (σ_{back}) which is accommodated mainly by elastic strains (Fig 4.13a). σ_{back} may reach the yield strength of the aggregate, triggering the production of dislocations. Dislocation tangling is partly counteracted by limited dynamic recovery, mostly along existing grain boundaries. At the margins of the tip damage zones ('1' in Fig. 4.13), stresses rise, accelerating the production of dislocations and hence leading to work hardening. Dislocation tangles exert a backstress to values exceeding the fracture strength, causing the formation of intragranular microfractures in Qtz and Plag. Work hardening decelerates ('2' in Fig. 4.13) as the length and number of microfractures increases (σ_{yield} in Fig. 4.13a). Intragranular fractures propagate and interconnect to form transgranular microshears (F-type shear zones).

The peak strength of the rock (σ_{fail}) is reached just prior to the intercon-

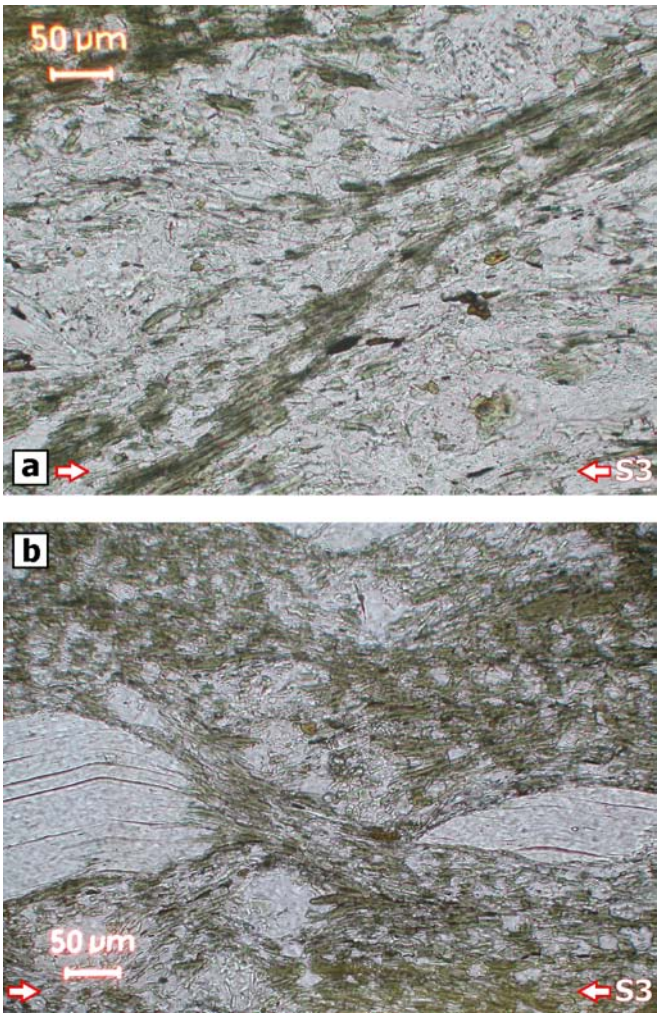

Figure 4.13: (a) Mylonitic microfabrics from sample CC01, showing a top-to-north shear band in S3. Green Bt2 is aligned within the shear band. Grain sizes are markedly reduced with respect to the pre-mylonitic host mineral. (b) Mylonitic microfabrics from sample CC52. Boudinaged Ms porphyroclast with fringes of green Bt2 forming in the boudin necks. Note small, uniform grain size of synmylonitic minerals. See text for further explanation.

nection of intragranular fractures (Fig. 4.13a). Most strain is accommodated by slip along transgranular microshears at this stage. However, coeval to the formation of microfractures ('2' in Fig. 4.13), Bt reacts syntectonically to fine-grained reaction products (Kerrich et al., 1980), and Qtz undergoes dynamic recovery and -recrystallization, further weakening the rock ('3' in Fig. 4.13). This enhanced deformability results in ductile deformation, which is

expressed by the rotation of S1/2 forming a ductile bead (Elliot, 1976, Fusseis et al., 2006). Microfractures create pathways for fluids, which further decrease rock strength by increasing pore-fluid pressure (thus decreasing effective normal stress on fracture surfaces) and/or by enhancing hydrolytic weakening (Griggs & Blacic, 1965, Hartley & Wilshaw, 1973, Hirth & Tullis, 1992). Incompatible deformation at grain boundaries due to enhanced dislocation glide on the basal planes of Bt in S2 may trigger brittle failure in adjacent Qtz or Plag grains (Gottschalk et al., 1990, Shea & Kronenberg, 1993, Holyoke & Tullis, 2006a&b).

Transgranular microshears and macroscopic F-type shear zones (fractures) are transient phenomena during strain localization and with increasing strain and percentage of dynamically recrystallized and newly grown fine-grained minerals, fractures accommodate a smaller proportion of the bulk strain ('4' in Fig. 4.13). Few microfractures form at this stage and fault rock in microshears recrystallizes dynamically. Strain is partitioned between slip on discrete fractures, distributed shearing and the synkinematic reaction of Bt1. With ongoing deformation all Qtz1 grains are dynamically recrystallized and most primary Bt1 has reacted. Dislocation creep replaces fracturing as the dominant (i.e., strength-controlling) deformation mechanism. The strength of the mylonite evolves gradually towards a stable value (σ_{stead}) as steady-state microfabrics form ('5' in Fig. 4.13).

4.6 Conclusions

The investigation of strain localization in the Cap de Creus "Northern shear belt" has shown that crack-like discontinuities in tip damage zones of mylonitic shear zones formed by fracturing. Transient synmylonitic stages of brittle failure and slip along fractures were identified as integral in the propagation of mylonitic shear zones. This is consistent with the notion previously presented in Fusseis et al. (2006) that the brittle-viscous transition is strain-dependent.

In detail, propagation of mylonitic shear zones in all metasedimentary country rocks was accommodated by intra- and transgranular fracturing together with distributed dislocation creep in Qtz and Bt as well as retrograde reaction of the latter. The relative activity of these deformation mechanisms varies with increasing strain and thereby does their contribution to strain ac-

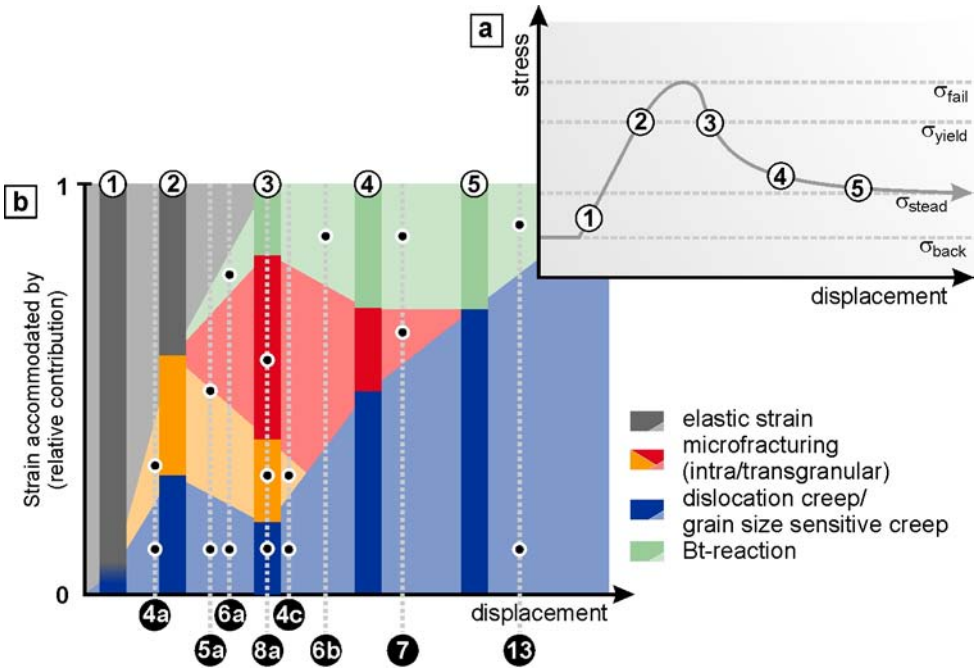

Figure 4.14: Model for the evolution of a propagating mylonitic M-type shear zone. (a) Strength evolution of shear zone during its propagation. (b) Relative contribution of deformation mechanisms during propagation of the mylonitic M-type shear zone. See text for explanation. White labels correspond to positions within the ductile tip damage zone shown in Fig. 4.2. Black labels refer to microstructures shown in previous figures. The dominant deformation mechanisms that can be seen in these figures are indicated by black circles.

commodation. Low strain increments involve predominant work hardening and intragranular fracturing. With increasing strain, transgranular fractures form and localize deformation, while the reaction of Bt1 to Bt2, Ms2, Chl and Ilm and the dynamic recrystallization of Qtz progress. After a critical amount of shearing (shear strain $\gamma \sim 1$), dynamically recrystallized Qtz and neoblasts of Bt2, Ms2, Ilm and Chl form a rheologically weak matrix that accommodates all of the deformation.

Fractures orientationed subparallel or antithetically with respect to the mylonitic shearing plane are attributed to the influence of existing foliation. In particular, the fracture orientation was shown to depend on the amount, distribution and orientation of cleavage domains (consisting mainly of biotite) and microlithons (dominated by quartz) in the rock. High biotite contents, good alignment and high cleavage domains/microlithons ratios

favour the propagation of fractures propagation in directions rotated up to 90° anticlockwise with respect to the shearing plane. The influence of the existing foliation on the orientation of propagating fractures explains the basic sigmoidal geometries that characterize shear zone networks at the Cap de Creus (e.g. Carreras, 2001).

4.7 Acknowledgements

We thank Claudio Rosenberg, Matthias Konrad-Schmolke, Patience Cowie and the participants of a field trip in May of 2006 for stimulating discussions. Furthermore we thank Sarah Hauten and Susanne Schneider for their assistance during preparation of the manuscript. We acknowledge the support of the Cap de Creus national park authorities for issuing a permit to collect rock samples in the park and thank Jordi Carreras for his help. This work was funded by DFG project Ha 2403/6.